

## Article

# Experimental Studies on the Phase Separation Behavior of Molten Benzenesulfonate-Modified PET/PA6 Blends

Xiao-Jun Ma<sup>1,2</sup>, Qi-Yu Ye<sup>1,2</sup>, Shao-Jie Zheng<sup>1,2</sup> , Ji-Jiang Hu<sup>1,2</sup> and Zhen Yao<sup>1,2,\*</sup><sup>1</sup> State Key Laboratory of Chemical Engineering, Zhejiang University, Hangzhou 310027, China<sup>2</sup> Institute of Polymerization and Polymer Engineering, Zhejiang University, Hangzhou 310027, China

\* Correspondence: yaozhen@zju.edu.cn

**Abstract:** In this work, nylon 6 (PA6) and cationic dyeable polyester (CDP) modified with benzenesulfonate groups were reactively blended in a twin-screw extruder. The well-mixed CDP/PA6 blends were re-molten and statically kept for various amounts of time. The morphology evolution caused by phase separation was observed by a scanning electron microscope (SEM) and an atomic force microscopy-infrared (AFM-IR) technique. In the absence of shear force, the homogeneously mixed blends were found to separate rapidly into two phases because of the poor miscibility between polyester and polyamide. In the early stage, the dispersed phase was small in size and irregular in shape. With prolongation of the phase separation time, the dispersed phase turned into larger and spherical particles to minimize the interface between phases. The phase separation process typically lasted 2 to 7 min. This means that the effects of phase separation on the morphology of the blends cannot be ignored in injection molding, compression molding, or other processing processes short of shear force. The effects of the ratio between polyester and polyamide, the benzenesulfonate content, and the molecular weight of polymers on phase separation behavior were investigated.

**Keywords:** CDP; PA6; reactive blends; phase separation; influencing factors



**Citation:** Ma, X.-J.; Ye, Q.-Y.; Zheng, S.-J.; Hu, J.-J.; Yao, Z. Experimental Studies on the Phase Separation Behavior of Molten Benzenesulfonate-Modified PET/PA6 Blends. *Macromol* **2023**, *3*, 54–64. <https://doi.org/10.3390/macromol3010005>

Academic Editor: Ana María Díez-Pascual

Received: 10 December 2022

Revised: 11 January 2023

Accepted: 16 January 2023

Published: 31 January 2023



**Copyright:** © 2023 by the authors. Licensee MDPI, Basel, Switzerland. This article is an open access article distributed under the terms and conditions of the Creative Commons Attribution (CC BY) license (<https://creativecommons.org/licenses/by/4.0/>).

## 1. Introduction

Polyethylene terephthalate (PET) and polyamide 6 (PA6) are two types of widely used polymer materials, with annual outputs in the tens of millions of tons [1]. PET has the advantages of low cost, high rigidity, good creep resistance, and dimensional stability. However, impact resistance, wear resistance, and antistatic properties of PET need to be improved [2,3]. PA6 has excellent impact resistance and antistatic properties, but it has high processing shrinkage and high cost [4–6]. PET/PA6 blends are expected to combine the advantages of these two types of polymers and improve the overall performance. However, this expectation is difficult to achieve due to the poor miscibility between PET and PA6. In recent years, many studies have been devoted to improving the compatibility between polyester and polyamide. Typical approaches involved the in situ production of the compatibilizers, which are amphiphilic and miscible with both polyester and polyamide [7–13].

One approach is to generate a polyester–polyamide block copolymer through the ester–amide exchange reaction between polyester and polyamide. Typically, a catalyst, such as *p*-toluenesulfonic acid (TsOH), is employed to promote ester–amide exchange. Pillon et al. carried out melt blending of PET and PA66 in the Brabender mixer and twin-screw extruder with 0.2 wt% TsOH [7]. The structure of the product characterized by <sup>13</sup>C NMR showed that TsOH was an effective catalyst for the ester–amide exchange reaction in the PET/PA66 melt-blending system. Evstatiev et al. prepared a PET/PA6/PA66 ternary blend with TsOH as a catalyst to improve the compatibility and mechanical properties of the blend [8]. A series of test results showed that block copolymers were generated and had the effect of in situ compatibilization on the blend. Yao et al. added TsOH to a blend of poly(butylene succinate) (PBS) and poly(hexamethylene (*iso-co-tere*)phthalamide)

(PA6IcoT) and carried out transesterification in a horizontal reactor [8]. Quantitative analysis validated that TsOH was an effective catalyst for the transesterification reaction to generate sufficient copolymers to improve the compatibility of PBS and PA6IcoT. Samperi et al. conducted a quantitative analysis on the transesterification reaction of the PA6/PBT blend system [14]. The results revealed that only the carboxyl end groups of PBT and PA6 were able to react in the initially biphasic PA6/PBT blends so that an outer-inner exchange took place. Block copolymers can also be generated through a chain-extension method involving the reaction between the chain extender and the end groups of polyester and polyamide. Most of the employed reactions are irreversible reactions with fast rates and exclusion of the generation of small molecules. Commonly used chain extenders include epoxy compounds, dioxazolines, and diisocyanates [10,15]. The addition of ionomers can also enhance the compatibility of polyester and nylon. The ionomer structure contains a small number of ionic groups, which can introduce special ionic interactions between the two polymers during blending, thereby achieving a compatibilizing effect. Ju et al. used the phosphonate poly(ethylene terephthalate) ionomer to modify the compatibility of the immiscible amorphous polyester (PETG) and semi-crystalline polyamide (poly(isophthalate adipyl) methylamine) (MXD6) [11,12]. The research group also studied the influence of the phosphonate poly(ethylene terephthalate) ionomer on the compatibility of the blend of PET and MXD6. The characterization results of the product showed that the size of the phase separation in MXD6 decreased with the increase of the ionic monomer concentration [13].

However, the morphology of the polymer blends is a quasi-steady-state structure. In injection molding, compression molding, and other processing processes, melting blends undergo a low shear rate or even a static state. The two incompatible phases undergo phase separation driven by the thermodynamical instability [16]. Most studies focused on the phase separation of polymer solutions induced thermally and/or by the evaporation of solvents [17–22]. There are a few related studies on phase morphology evolution of polymer blends under molten conditions. Zhong et al. prepared isotactic polypropylene (iPP)/ethylene-octene random copolymer (EOC) and iPP/ethylene-octene block copolymer (OBC) blends of different compositions using a solution-precipitation method. To study phase separation, the blends were annealed at 200 °C for various durations and were investigated quantitatively using an in situ atomic force microscopy-infrared (AFM-IR) technique. The compatibility of OBC with iPP was found to be better than that of EOC [23]. Moonprasith et al. prepared polymer blends of bisphenol-A polycarbonate and poly(methyl methacrylate) (PMMA) using a pressure-driven capillary rheometer. A large amount of PMMA was found on the surface of the strand extruded from the rheometer. The segregation behavior was enhanced by higher temperatures, higher shear rates, and lower molecular weight of PMMA [24]. Chuang et al. investigated the competitive effects of the hydrogen-bonding interaction and molecular weight on the phase and crystallization behaviors of polystyrene-block-poly(ethylene oxide) (PS-b-PEO)/polystyrene-block-poly(acrylic acid) (PS-b-PAA) blends. The hydrogen-bonding interaction between the two polymer chains enabled the block copolymers to co-organize into common PS and PEO/PAA microdomains, leading to improved miscibility [25].

In our previous work, a series of polyester/PA6 blends were prepared in a twin-screw extruder using PA6 and benzenesulfonate-modified PET (commercially named CDP) [26]. It was found that the compatibility between CDP and PA6 was considerably better than that of PET and PA6. In this work, the well-mixed CDP/PA6 blends were re-molten and statically kept for various amounts of time to induce phase separation. The morphology evolution caused by the phase separation was studied. The effects of the ratio between polyester and polyamide, the benzenesulfonate content, and the molecular weight of polymers on phase separation behavior were investigated.

## 2. Materials and Methods

### 2.1. Materials

The CDP and PA6 used in this work are summarized in Tables 1 and 2. Formic acid was supplied by China National Chemicals Co., Ltd. (Shanghai, China).

**Table 1.** CDP and PET used in this work.

CDP	Molecular Weight (g/mol)	Sulfonic Acid Content (mol %)	Supplier
PET	18,400	0	Zhejiang Henglan Technology Co., Ltd.
LC2	14,500	2.0	Zhejiang Henglan Technology Co., Ltd.
LC4	11,700	4.0	Zhejiang Henglan Technology Co., Ltd.
LC8	11,400	8.0	Self-made
MC4	23,000	4.0	Self-made
HC4	25,400	4.0	Self-made

**Table 2.** PA6 used in this work.

PA6	Molecular Weight (g/mol)	Supplier
LA	19,600	Zhejiang Henglan Technology Co., Ltd.
MA	31,600	Ube Co., Ltd., Thailand
HA	39,700	Ube Co., Ltd., Thailand

### 2.2. Preparation of Polyester/Nylon Blends

CDP and PA6 were vacuum dried at 100 °C for 12 h before being mixed uniformly and melt-extruded to prepare a series of CDP/PA6 blends. The melt extrusion was carried out in the HAKKE PolyLab OS instrument with RheoDrive 7 as the driving system and Rheomex PTW 16/40 OS as the twin-screw extrusion unit (TSE). The main screw had an L/D ratio of 40 and a rotation speed of 300 r/min. The residence time was about 3 min. Table 3 provides the extrusion temperature, composition ratios, and sample designations of the prepared blends.

**Table 3.** Reactive extrusion conditions.

Sample	Temperature (°C)	CDP	PA6	CDP Content (wt%)	PA6 Content (wt%)
LC2/LA(70/30)	250	LC2	LA	70	30
LC4/LA(70/30)	250	LC4	LA	70	30
LC8/LA(70/30)	250	LC8	LA	70	30
LC4/LA(50/50)	250	LC4	LA	50	50
LC4/LA(30/70)	250	LC4	LA	30	70
LC4/MA(70/30)	250	LC4	MA	70	30
LC4/HA(70/30)	250	LC4	HA	70	30
MC4/LA(70/30)	250	MC4	LA	70	30
HC4/LA(70/30)	250	HC4	LA	70	30
PET/LA(70/30)	250	PET	LA	70 (PET content)	30

### 2.3. Phase Separation Experiment

The dried CDP/PA6 blend in the shape of flakes was placed in a mold and heated by a hot press (model GT-7014-A50C) to 260 °C. No pressure was applied to the samples to avoid significant changes in the shape of sample. In order to obtain samples with various degrees of phase separation, the molten blends were kept at 260 °C statically for 1, 2, 3, 5, 7, 10, or 20 min before being rapidly cooled down to room temperature to maintain the morphology.

## 2.4. Characterization Method

### 2.4.1. Nuclear Magnetic Resonance ( $^{13}\text{C}$ NMR)

A 500MHZ BRUKER-AVANCE 400 nuclear magnetic resonance spectrometer was used for  $^{13}\text{C}$  NMR analysis. Deuterated trifluoroacetic acid ( $\text{CF}_3\text{COOD}$ ) was used as the solvent with tetramethylsilane (TMS) as the internal standard. The number of scans was 3000. The following samples were characterized with NMR: LC2/LA(70/30), LC4/LA(70/30), LC8/LA(70/30), and PET/LA(70/30).

### 2.4.2. Scanning Electron Microscope (SEM)

The morphology of the blends was observed using a Hitachi SU-8010 field emission scanning electron microscope (SEM). Before observation, the samples were quenched in liquid nitrogen and etched in formic acid for 48 h to remove the PA6-riched phase in the blends. The etched samples were vacuum dried at 80 °C for 4 h. The samples were adhered to the observation deck with conductive glue and treated with Pt spraying for 120 s. All samples were characterized with SEM.

### 2.4.3. Atomic Force Microscopy-Infrared (AFM-IR)

The Bruker nanoIR2-fs multifunctional nano-infrared spectrometer was used for AFM-IR experiments. The topography of the sample was scanned with a PR-EX-nIR2-5 probe, and the sample was irradiated with a mid-infrared quantum cascade tunable pulsed laser MIRcat QCL with a wavenumber range of 950–1900  $\text{cm}^{-1}$ . In this experiment, the C=O stretching vibration peak (1720  $\text{cm}^{-1}$ ) was used as the characteristic peak to obtain the distribution of the polyester phase in the blends. LC4/LA(50/50) were characterized with AFM-IR.

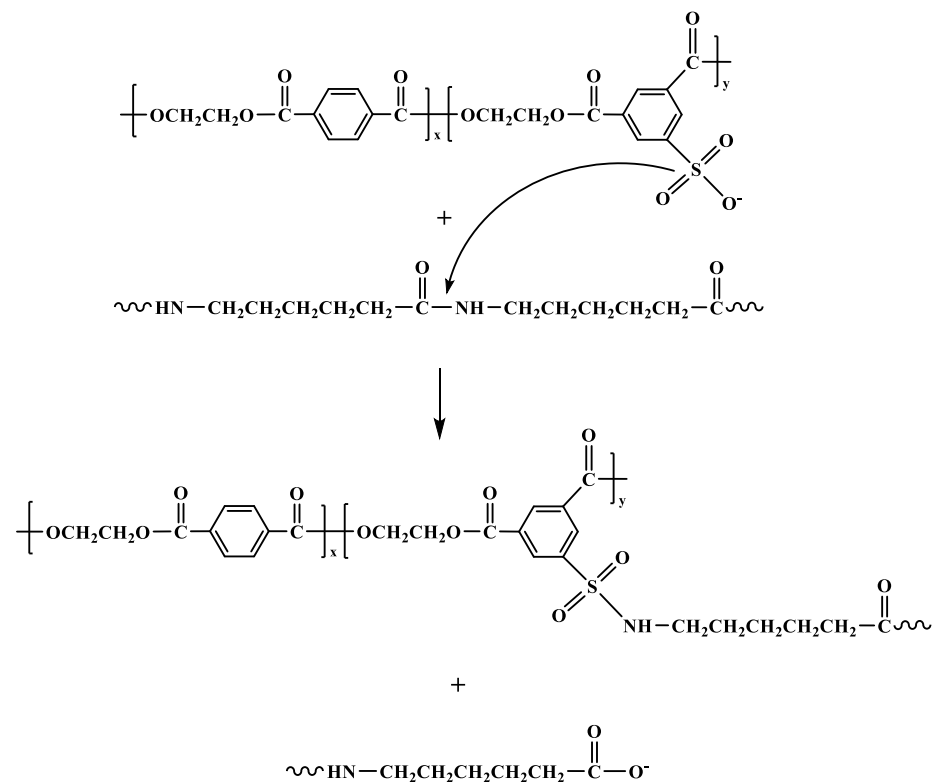
### 2.4.4. High-Pressure Capillary Rheology

Rheological tests were performed by using Malvern RH10 Capillary Rheometers. The samples were preheated at 250 °C, 260 °C, 265 °C, and 280 °C for 1 min. The shear viscosity of the sample was measured in the shear rate range of 100–3000  $\text{s}^{-1}$ . All raw materials listed in Tables 1 and 2 were characterized by the capillary rheometer.

## 3. Results and Discussion

In previous studies, it has been found that benzenesulfonate is an efficient catalyst for ester–amide exchange. During the melt-extrusion process of CDP and PA6, the benzenesulfonate group on the CDP molecular chain attacks the amide bond (-NHCO-) in PA6, resulting in an exchange reaction and the formation of a polyester/polyamide graft copolymer as shown in Scheme 1 [23]. The produced graft copolymer acts as a compatibilizer to facilitate the mixing of CDP and PA6.

An AFM-IR image of LC4/LA(50/50) is presented in Figure 1a. The distribution of polyester phase in the samples is characterized by the intensity of the IR signal at the specific wavenumber. In this work, the peak at 1720  $\text{cm}^{-1}$ , which corresponds to the stretching vibration of the C=O linked to the benzene rings of CDP, was chosen as the characteristic wavenumber. The yellow zone is the fraction with a strong IR signal, which is identified as the polyester-rich phase. The auburn zone is the fraction with a negative signal, which is identified as the PA6-rich phase. The orange area corresponds to the 0 V signal and is the region with an equal amount of polyester and nylon mixed at a scale smaller than the spatial resolution of IR (10 nm). As shown in Figure 1a, LC4/LA(50/50) exhibited a co-continuous phase morphology. The yellow PET-rich fraction and the auburn mixture of PET/PA6 each formed a continuous phase. A few blue PA6-rich particles with irregular shape were dispersed in the auburn phase. The thickness of each continuous phase and the size of particles were both smaller than 1  $\mu\text{m}$ . Therefore, it can be concluded that CDP and PA6 were well mixed at the weight ratio of 50:50 through melting extrusion in TSE. The morphology of LC4/LA(50/50) was further confirmed by Figure 1b, which presents the SEM image of LC4/LA(50/50) etched with formic acid.



**Scheme 1.** Reaction between CDP and PA6.

However, after the samples were molten and statically kept for various durations, the well-mixed morphology changed as shown in Figure 1c–h. After the blend was left in the molten state statically for 1 min, more dispersed particles emerged from the continuous PA6-rich phase. The size of the PA particles was much smaller than 1  $\mu\text{m}$ , which is the result of reduced interfacial tension between the CDP and PA6 phases with the presence of the graft polymer. For the same reason, the shape of the dispersed particles did not need to be spherical to maintain the smallest specific surface area. The total volume of the dispersed phase was less than 50%, which was the overall fraction of PA6 in the sample LC4/LA(50/50). After two minutes of phase separation, the volume of the dispersed phase gradually increased. Particles with a size greater than 1  $\mu\text{m}$  appeared. With the extension of the statically melting time to 5 min, the proportion of the etched PA6-rich phase increased to nearly 50%. The residual CDP-rich phase demonstrated irregular shapes. With further increase in the phase separation, the specific surface area of the CDP-rich phase began to decrease. After 10 min, the CDP-rich phase became spherical. From the above observation, it can be seen that the co-continuous phase of the extruded sample, LC4/LA(50/50), was a thermodynamically unstable state, which quickly changed into the morphology of a traditional incompatible blend once it was statically molten. In the following sections, the effects of polymer ratios, content of benzenesulfonate in CDP, and polymer molecular weight on the phase separation process were investigated.

Figures 2 and 3 show the phase morphological evolution of two samples: LC4/LA(30/70) and LC4/LA(70/30). It can be seen from Figures 2a and 3a that both samples were uniformly dispersed as extrudes directly out of the TSE. In LC4/LA(30/70), the PA6-rich phase was expected to be the continuous phase and to be dissolved by formic acid. However, the sample with zero phase separation time (Figure 3a) maintained a complete continuous morphology after being etched by formic acid. After one minute of phase separation, the etched residue consisted of the accumulation of numerous irregular particles with dimensions less than 1  $\mu\text{m}$ . With the prolongation of phase separation time, the fraction of material etched away increased. When the phase separation time exceeded 5 min, the residual PET-rich phase condensed into micron-sized particles, which gradually approached a spherical shape. After 10 min, the

remaining PET particles were fully spherical with diameters between 1 and 10 microns. In LC4/LA(70/30), a large number of pores left by the etching of the PA6-rich phase appeared after one minute of phase separation. The pores were irregular in shape and had a wide size distribution of scales between 0.1 and 10  $\mu\text{m}$ . With increasing phase separation time, the number of pores increased, and the shape became more regular. After being statically molten for 5 min, a large number of pores with a shape close to spherical and uniform size appeared. In this paper, the time of the appearance of spherical pores/particles was defined as the phase separation point, which was 5, 5, and 7 min for the three samples, LC4/LA(30/70), LC4/LA(50/50), and LC4/LA(70/30), respectively.

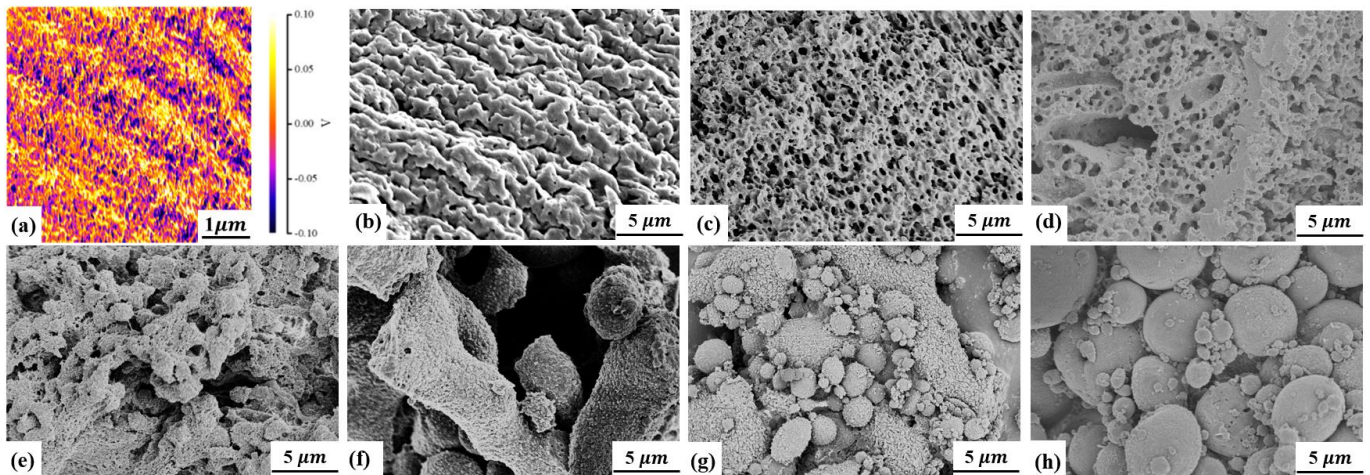


**Figure 1.** Morphology evolution of LC4/LA(50/50) after being statically molten for various durations: (a) 0 min, directly out of the TSE (AFM-IR image); (b) 0 min, directly out of the TSE (SEM image); (c) 1 min; (d) 2 min; (e) 3 min; (f) 5 min; (g) 7 min; (h) 10 min.

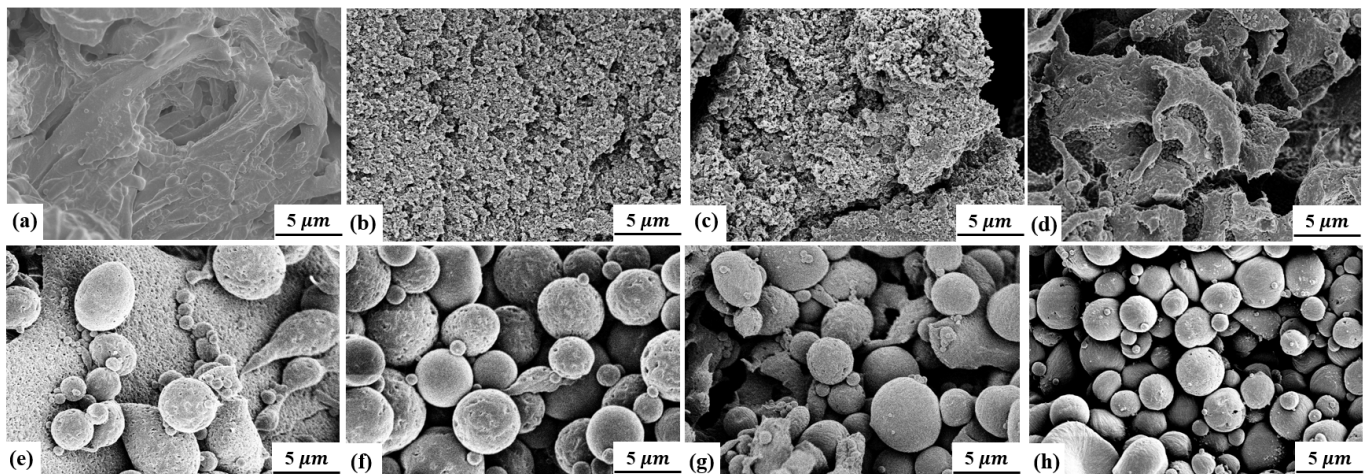


**Figure 2.** Phase evolution of LC4/LA(30/70) after being statically molten for various durations: (a) 0 min, directly out of the TSE; (b) 1 min; (c) 2 min; (d) 3 min; (e) 5 min; (f) 7 min; (g) 10 min; (h) 20 min.

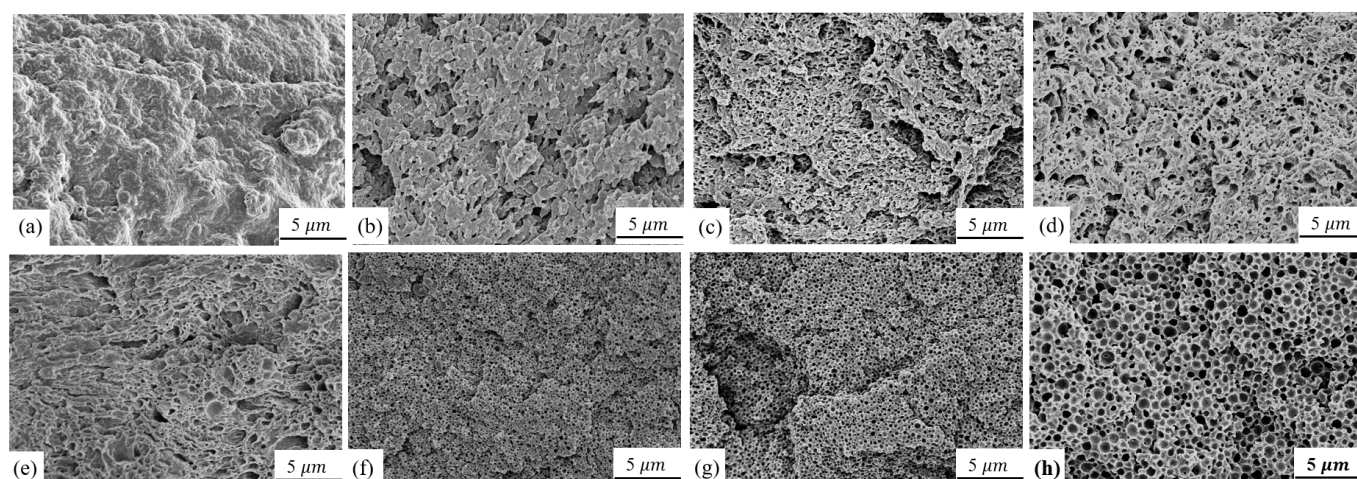


**Figure 3.** Phase evolution of LC4/LA(70/30) after being statically molten for various durations: (a) 0 min, directly out of the TSE; (b) 1 min; (c) 2 min; (d) 3 min; (e) 5 min; (f) 7 min; (g) 10 min; (h) 20 min.

The phase separation point was also affected by the benzenesulfonate content in CDP. The molecular fraction of benzenesulfonate in LC2, LC4, and LC8 were 2.0, 4.0, and 8.0%, respectively. The phase separation processes of LC2/LA(70/30) and LC8/LA(70/30) were similar to that of LC4/LA(70/30). However, the phase separation point of LC2/LA(70/30) was at 3 min, which is significantly less than the 7 min for LC4/LA(70/30) and LC8/LA(70/30).

The size distribution of the dispersed phase after phase separation for 7 min are shown in Figure 4 for these three samples. The diameter of the dispersed phase of LC2/LA(70/30) was in the range of 0.3–1.20  $\mu\text{m}$  with an average size at 0.70  $\mu\text{m}$ . The dispersed phase of LC4/LA(70/30) and LC8/LA(70/30) had smaller average diameters of 0.34 and 0.28  $\mu\text{m}$ , respectively. The dispersed phase distributed in the range of 0.1–0.7  $\mu\text{m}$  and 0.1–0.5  $\mu\text{m}$  for LC4 and LC8 samples, respectively.

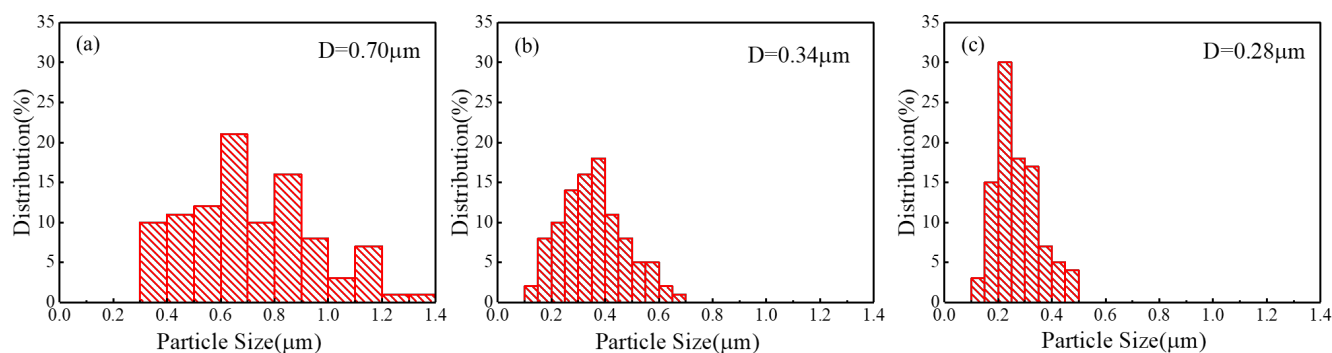


**Figure 4.** Size distribution of dispersed phase at stationary melting for 7 min: (a) LC2/LA(70/30); (b) LC4/LA(70/30); (c) LC8/LA(70/30).

These results show that with the increase of benzenesulfonate content, the phase separation point was delayed, and the size of the dispersed phase decreased after the phase separation. This is related to the amount of graft copolymer formed during the reactive blending process. Figure 5 is the NMR spectra of these three samples and PET/LA(70/30). The chemical shifts corresponding to C-a and C-b of CDP were in the range of 64–63 ppm. This characteristic peak appeared in the formic acid soluble fraction of the CDP/PA6 blends, indicating that part of the polyester was grafted onto PA6 and dissolved by formic acid together with PA6. This phenomenon was not found in PET/LA(70/30). The C-c attached to the amino group in PA6 had a chemical shift at 42–41 ppm, which was chosen as the comparison for the quantitative calculations of the peak areas of C-a and C-b. The results show that the peak areas of C-a and C-b for LC2/LA(70/30), LC4/LA(70/30), and LC8/LA(70/30)

were 0.05, 0.10, and 0.11, respectively. It proved that when the content of benzenesulfonate increased from 2.0 mol% to 4.0 mol%, the amount of graft copolymer increased. Therefore, the phase stability of the blends was increased, and the size of the dispersed phase was decreased. When the content of benzenesulfonate was further increased to 8.0 mol%, the resulting graft copolymer did not increase. The reason is analyzed as follows: LC4 and LC8 have an average of 2.3 and 4.5 benzenesulfonates attached to each polymer chain, respectively. Due to the incompatibility of CDP and PA6, the polymer chains were in a coiled state in the molten blends. Fractions of benzenesulfonate groups are embedded within the CDP chains and cannot participate in the reaction. Therefore, within a certain range, by increasing the content of benzenesulfonate in the CDP, the amount of generated graft copolymer can be increased, and the stability of the blend in the molten state can be improved. However, the average number of benzenesulfonates on each CDP chain is over two, and further increase in benzenesulfonate content would not lead to additional benefits.

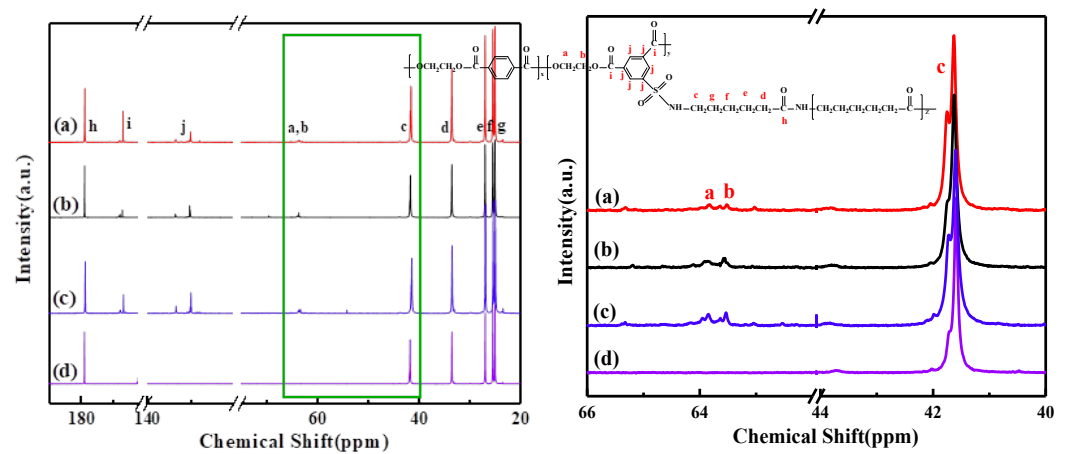


**Figure 5.**  $^{13}\text{C}$  NMR diagram of the amount of graft copolymers formed in the range of 66–40 ppm: (a) LC2/LA(70/30); (b) LC4/LA(70/30); (c) LC8/LA(70/30); (d) PET/LA(70/30).

Blends of CDP and PA6 with various molecular weights were prepared and subjected to phase separation by being statically molten. The size distribution of the dispersed phase was shown in Figure 6. Here, LC4, MC4, and HC4 are CDP with 4 mol% benzenesulfonate and a molecular weight of 11,700, 23,000, and 25,400, respectively. LA, MA, and HA are PA6 with a molecular weight of 19,600, 31,600, and 39,700, respectively. In the process of melt blending and melt phase separation, the effects of polymer molecular weight are reflected by the difference in melt viscosity. During melt blending processes, the counteraction of shear force and interfacial tension determines the size of the dispersed phase. Wu et al. studied the blending of PA6 and ethylene-propylene rubber and derived an empirical formula to determine the size of the dispersed phase [24].

$$D = \begin{cases} \frac{4\sigma\eta_r^{0.84}}{\gamma\eta_m} \Big| \eta_r \geq 1 \\ \frac{4\sigma\eta_r^{-0.84}}{\gamma\eta_m} \Big| \eta_r < 1 \end{cases} \quad (1)$$

where  $\sigma$  is the interfacial tension between two polymer melts;  $\gamma$  is the shear viscosity;  $\eta_m$  is the viscosity of the matrix phase; and  $\eta_r$  is the ratio between the viscosity of the dispersed phase and the matrix phase.

This formula shows that the more the viscosity ratio of the two phases deviates from one, the greater the interfacial tension of the system, and the larger the size of the resulting dispersed phase. During static melting processes, viscosity also causes differences in the diffusivity of polymer molecules, which in turn affects the formation of the dispersed phase. In the following discussion, the influence of molecular weight on phase separation behavior is discussed in terms of the difference in the viscosity of each polymer melt.

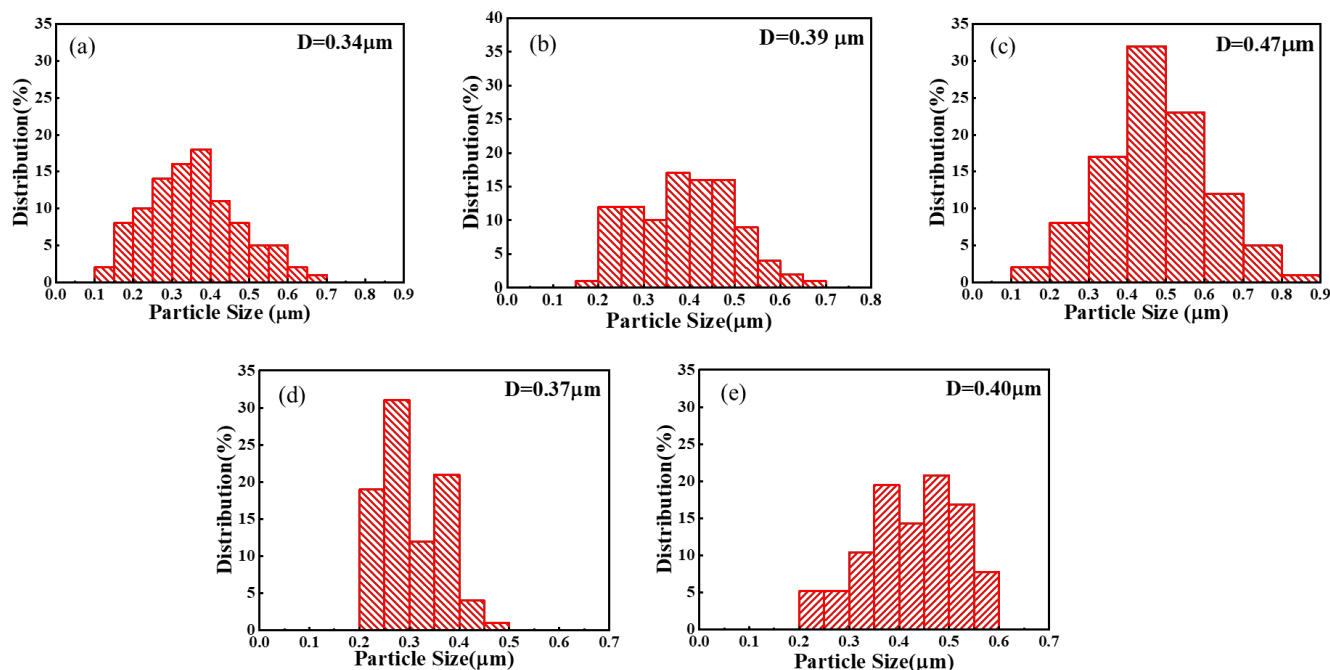


**Figure 6.** Influence of molecular weight on size distribution of the dispersed phase: (a) LC4/LA(70/30); (b) LC4/MA(70/30); (c) LC4/HA(70/30); (d) MC4/LA(70/30); (e) HC4/LA(70/30).

The melt viscosity of each polymer at different shear rates was measured using a high-pressure capillary rheometer. The ratio of dispersed phase viscosity to matrix phase viscosity in each blend is shown in Figure 7. The higher the shear rate, the closer the viscosities of CDP and PA6 were. The viscosity of LA was smaller than that of LC4. With the increase of  $\gamma$  from 100 to 1000  $\text{s}^{-1}$ , the viscosity ratio between LA and LC4 increased from 0.7 to 0.9. The viscosity of MA and HA were both larger than LC, and the viscosity difference was large. In the  $\gamma$  range of 100 to 1000  $\text{s}^{-1}$ , the viscosity ratio of MA/LC4 was decreased from 1.7 to 1.5, and that the viscosity ratio of HA/LC4 was decreased from 3.9 to 2.6. While the viscosity of LA was much smaller than that of MC4 and HC4, the viscosity ratios of LA/MC4 and LA/HC4 were increased from 0.4 to 0.7 and from 0.3 to 0.5 in the  $\gamma$  range of 100 to 1000  $\text{s}^{-1}$ , respectively.

Combining these rheological data with the phase separation results, it can be found that the closer the viscosity of the dispersed phase and the matrix phase was, the longer the phase stabilization time was. The LC4/HA(70/30) and HC4/LA(70/30), whose viscosity ratio deviated by a maximum of one, had the shortest phase stabilization times. Between these two blends, the size of the dispersed phase in HC4/LA(70/30) was smaller. HC4/LA had higher matrix viscosity, which may suppress the diffusion of PA6 out of the matrix and lead to a smaller dispersed phase.

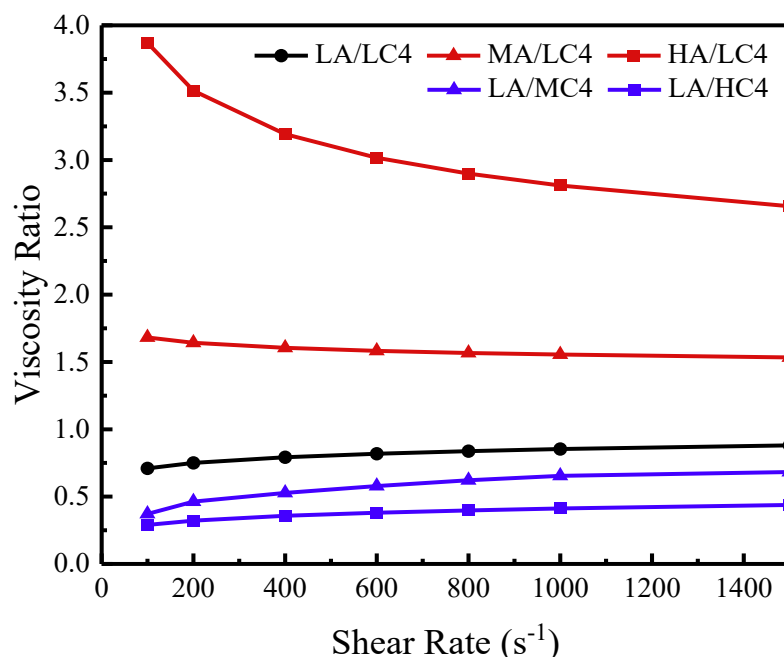


**Figure 7.** The melt viscosity of CDP and PA6 raw materials varies with the shear rate at 250 °C.

#### 4. Conclusions

In this work, the phase separation process of CDP/PA6 blends was observed by AFM-IR and SEM. The molten blends were statically kept at 260 °C for various durations to induce the phase separation. Without shear force, the homogeneously mixed blends rapidly separated into two phases. In the early stage, the dispersed phase consisted of small and irregular particles. With the increase in phase separation time, the dispersed phase turned into larger and spherical particles to minimize specific surface area. The phase separation process typically lasted 2 to 7 min.

Increasing the benzenesulfonate content would increase the amount of in situ-produced compatibilizer and improve the stability of the blend in the molten state. The effects of molecular weights of CDP and PA6 were reflected by the difference in the melt viscosity of each polymer. The closer the melt viscosity of the dispersed phase and the matrix phase was, the longer the phase stabilization time was.

The findings of this work show that although two incompatible polymers can be mixed homogeneously with the help of in situ-generated compatibilizers, the blends were still in a thermodynamically unstable state. If the blends were re-molten in the absence of shear force, the two incompatible polymers rapidly separated into two phases, resulting in changes in morphology and even properties.

**Author Contributions:** Z.Y. and J.-J.H.: Conceptualization, Methodology, Investigation, and Writing—review and editing. X.-J.M. and Q.-Y.Y.: Investigation, Data curation, and Writing—original draft. S.-J.Z.: Investigation and Writing—editing. All authors have read and agreed to the published version of the manuscript.

**Funding:** This research received no external funding.

**Data Availability Statement:** The authors declare that the main data supporting the findings and conclusions of this study are available within the article. Original and additional data are available from the corresponding author upon request.

**Conflicts of Interest:** The authors declare no conflict of interest.

## References

1. Li, C.; Zhao, R.; Lu, X.D. 2019 Review and 2020 outlook for world and china synthetic fiber industry. *Pet. Petrochem. Today* **2020**, *28*, 14–17.
2. Nisticò, R. Polyethylene terephthalate (PET) in the packaging industry. *Polym. Test.* **2020**, *90*, 106707. [[CrossRef](#)]
3. d'Ambrières, W. Plastics recycling worldwide: Current overview and desirable changes. *Field Actions Sci. Rep. J.* **2019**, *19*, 12–21.
4. Anstey, A.; Codou, A.; Misra, M.; Mohanty, A.K. Novel compatibilized nylon-based ternary blends with polypropylene and poly (lactic acid): Fractionated crystallization phenomena and mechanical performance. *ACS Omega* **2018**, *3*, 2845–2854. [[CrossRef](#)] [[PubMed](#)]
5. Ksouri, I.; De Almeida, O.; Haddar, N. Long term ageing of polyamide 6 and polyamide 6 reinforced with 30% of glass fibers: Physicochemical, mechanical and morphological characterization. *J. Polym. Res.* **2017**, *24*, 1–12. [[CrossRef](#)]
6. Huang, S.; Toh, C.L.; Yang, L.; Phua, S.; Zhou, R.; Dasari, A.; Lu, X. Reinforcing nylon 6 via surface-initiated anionic ring-opening polymerization from stacked-cup carbon nanofibers. *Compos. Sci. Technol.* **2014**, *93*, 30–37. [[CrossRef](#)]
7. Pillon, L.; Utracki, L. Compatibilization of polyester/polyamide blends via catalytic ester-amide interchange reaction. *Polym. Eng. Sci.* **1984**, *24*, 1300–1305. [[CrossRef](#)]
8. Evstatiev, M.; Fakirov, S.; Schultz, J.; Friedrich, K. In situ fibrillar reinforced PET/PA-6/PA-66 blend. *Polym. Eng. Sci.* **2001**, *41*, 192–204. [[CrossRef](#)]
9. Yao, Z.; Sun, J.-m.; Wang, Q.; Cao, K. Study on ester–amide exchange reaction between PBS and PA6IcoT. *Ind. Eng. Chem. Res.* **2012**, *51*, 751–757. [[CrossRef](#)]
10. Néry, L.; Lefebvre, H.; Fradet, A. Polyamide–polyester multiblock copolymers by chain-coupling reactions of carboxy-terminated polymers with phenylene and pyridylene bisoxazolines. *J. Polym. Sci. Part A Polym. Chem.* **2005**, *43*, 1331–1341. [[CrossRef](#)]
11. Ju, L.; Pretelt, J.; Chen, T.; Dennis, J.M.; Heifferon, K.V.; Baird, D.G.; Long, T.E.; Moore, R.B. Synthesis and characterization of phosphonated Poly (ethylene terephthalate) ionomers. *Polymer* **2018**, *151*, 154–163. [[CrossRef](#)]
12. Ju, L.; Dennis, J.M.; Heifferon, K.V.; Long, T.E.; Moore, R.B. Compatibilization of polyester/polyamide blends with a phosphonated poly (ethylene terephthalate) ionomer: Comparison of monovalent and divalent pendant ions. *ACS Appl. Polym. Mater.* **2019**, *1*, 1071–1080. [[CrossRef](#)]
13. Ju, L.; Mondschein, R.J.; Vandenbrande, J.A.; Arrington, C.B.; Long, T.E.; Moore, R.B. Phosphonated Poly (ethylene terephthalate) ionomers as compatibilizers in extruded Poly (ethylene terephthalate)/Poly (m-xylylene adipamide) blends and oriented films. *Polymer* **2020**, *205*, 122891. [[CrossRef](#)]
14. Samperi, F.; Montaudo, M.; Puglisi, C.; Alicata, R.; Montaudo, G. Essential role of chain ends in the Ny6/PBT exchange. A combined NMR and MALDI approach. *Macromolecules* **2003**, *36*, 7143–7154. [[CrossRef](#)]
15. Xiao, L.; Wang, H.; Qian, Q.; Jiang, X.; Liu, X.; Huang, B.; Chen, Q. Molecular and structural analysis of epoxide-modified recycled poly (ethylene terephthalate) from rheological data. *Polym. Eng. Sci.* **2012**, *52*, 2127–2133. [[CrossRef](#)]
16. Kammer, H.; Kummerloewe, C.; Kressler, J.; Melior, J. Shear-induced phase changes in polymer blends. *Polymer* **1991**, *32*, 1488–1492. [[CrossRef](#)]
17. Sanviti, M.; Martinez-Tong, D.E.; Rebollar, E.; Ezquerro, T.A.; Garcia-Gutierrez, M.C. Crystallization and phase separation in PE-DOT:PSS/PEO blend thin films: Influence on mechanical and electrical properties at the nanoscale. *Polymer* **2022**, *262*, 13. [[CrossRef](#)]
18. Xiang, S.; Tang, X.X.; Rajabzadeh, S.; Zhang, P.F.; Cui, Z.Y.; Matsuyama, H. Fabrication of PVDF/EVOH blend hollow fiber membranes with hydrophilic property via thermally induced phase process. *Sep. Purif. Technol.* **2022**, *301*, 11. [[CrossRef](#)]
19. Wu, X.X.; Song, T.T.; Wei, Z.Z.; Shen, L.; Jiang, H.Q.; Ke, Y.B.; He, C.Y.; Yang, H.; Shi, W.C. Promoted liquid-liquid phase separation of PEO/PS blends with very low LiTFSI fraction. *Polymer* **2022**, *260*, 6. [[CrossRef](#)]
20. Kalourazi, S.F.; Wang, F.; Zhang, H.D.; Selzer, M.; Nestler, B. Phase-field simulation for the formation of porous microstructures due to phase separation in polymer solutions on substrates with different wettabilities. *J. Phys. Condens. Matter* **2022**, *34*, 16.
21. Tseng, Y.H.; Fan, Y.C.; Chang, C.T.; Lin, Y.L.; Chang, C.W.; Liao, C.W.; Chen, J.T. Photoinduced alignment under solvent vapor annealing (PA-SVA): Enhanced ordering and patterning in block copolymer films. *ACS Appl. Polym. Mater.* **2022**, *4*, 8536–8542. [[CrossRef](#)]
22. Pochivalov, K.V.; Basko, A.V. Formation of porous microspheres from semicrystalline polymer solutions: Diffusion-controlled and local phase separation. *Polym. Plast. Technol. Mater.* **2022**, *61*, 1279–1291.
23. Zhong, Z.X.; Peng, L.; Zhang, N.; Su, J.X.; Ye, N.B.; Luo, Z.F.; Han, C.C.; Huang, X.B.; Su, Z.H. Miscibility of isotactic polypropylene with random and block ethylene-octene copolymers studied by atomic force microscopy-infrared. *Polymer* **2022**, *259*, 10. [[CrossRef](#)]
24. Moonprasith, N.; Tatsumichi, M.; Nakamura, K.; Kida, T.; Tsubouchi, K.; Hiraoka, T.; Yamaguchi, M. Preparation of graded materials for miscible polycarbonate/poly(methyl methacrylate) blends by segregation under shear flow. *J. Appl. Polym. Sci.* **2023**, *140*, 8. [[CrossRef](#)]
25. Chuang, P.Y.; Liao, S.Y.; Wu, K.H.; Hu, Y.R.; Lo, C.T. Competitive Effects of Hydrogen Bonds and Molecular Weights on the Phase and Crystallization Behaviors of Binary Block Copolymers. *Macromolecules* **2022**, *55*, 7411–7424. [[CrossRef](#)]
26. Ma, X.J. Studies on the Preparation of PET/PA6 Alloy by Reactive Extrusion and Its Performance. Master's Thesis, Zhejiang University, Hangzhou, China, 2021.

**Disclaimer/Publisher's Note:** The statements, opinions and data contained in all publications are solely those of the individual author(s) and contributor(s) and not of MDPI and/or the editor(s). MDPI and/or the editor(s) disclaim responsibility for any injury to people or property resulting from any ideas, methods, instructions or products referred to in the content.